Chapter 7

Free-Piston Stirling Engine Generators

Songgang Qiu and Laura Solomon

Additional information is available at the end of the chapter

http://dx.doi.org/10.5772/intechopen.79413

Abstract

Free-Piston Stirling Engines (FPSEs) have recently attracted attention as a promising energy conversion technology because of their desirable characteristics such as high efficiency, high reliability, and easy and quiet operation. FPSE are truly a closed cycle system that works using variations in the internal pressure to drive the power piston that is connected to the reciprocating magnets in a linear alternator for energy conversion. The lack of manual linages and the use of clearance seals in a FPSE increase both the system's reliability and lifespan, as there is no contact or wear on the seals. These desirable attributes coupled with the fuel independence of FPSE makes them ideal candidates for use in remote power generation applications, particularly where maintenance is a high concern such as in NASA deep space missions, solar power generator, and combined heat and power systems. This chapter presents an introduction to FPSE along with a brief review of the underlying thermodynamics and Stirling cycle analysis. The general engineering analysis and numerical modeling approaches of Stirling engines will be discussed, followed by a section of engine design and efficiency calculations.

Keywords: free-piston Stirling engine, additive manufacturing, energy conversion, regenerator, heater head, CFD, thermal conduction losses, design optimization

1. Introduction

The continuing depletion of fossil fuel resources has led to the increase of global research into sustainable energy. This has resulted in the resurrection of the forgotten Stirling engine which is an external combustion engine unlike the more widely known Otto and Diesel engines which are internal combustion engines. One application where FPSE are gaining interest is in combined heat and power (CHP) because of its operation on a closed cycle, FPSE can be run on a variety of fuels such as solar [1], biogas [2], natural gas [3], waste gas [4] etc. Although

patented in 1816 by Robert Stirling, it would take the better part of a century for scientist to fully understand its complex physics [1]. The key to the high efficiency of the Stirling engine is what Stirling called an economizer but it more commonly referred to today as a regenerator [2]. The regenerator acts as a solid storage medium between the hot and cold heat exchangers. This allows for a reduction in the total amount of thermal energy input to the engine leading to an increase in the cycle efficiency. However, despite its numerous attractive qualities, historically the Stirling engine was replaced by theoretically inferior engines due to performance limitations resulting from the available materials of the time. The limitation on operating temperature is highly detrimental to the performance of a Stirling engine because the cycle efficiency is dependent on the temperature ratio and not the pressure ratio like in the Otto or Diesel cycles. However, the development of modern high-temperature superalloys has drastically increased the operational temperature of Stirling engines to nearly 1200 K. Research is ongoing to use cutting-edge manufacturing techniques such as additive manufacturing of metals to further increase the efficiency, improve the reliability, and reduce the manufacturing cost of the next generation of Stirling engines.

2. Thermodynamic cycle

An ideal Stirling cycle consists of four stages: (1) the working fluid, typically air, helium, or hydrogen, undergoes an isothermal expansion; (2) a constant-volume heat; (3) isothermal compression; and (4) constant volume heat addition. Regenerators play an important role in the cycle, as the heat stored in the regenerator during the early stage is recovered by the gas in the fourth stage. The efficiency of an ideal Stirling cycle approaches that of a Carnot cycle which depends only on the hot and cold temperatures. However, it is impossible to achieve an ideal cycle in a real system, and the actual efficiency of a Stirling engine is lower than the theoretical Carnot efficiency. State of the art Stirling engines have efficiencies near 40%.

3. Types of Stirling engines

The mechanical configurations of Stirling engines are generally divided into three groups: alpha, beta, and gamma [2]. In the alpha configuration the engine consists of two pistons that are housed in separate cylinders which are connected by the hot heat exchanger, regenerator, and cold heat exchanger. For alpha engines the pistons also act as the displacers. Both the beta and gamma engines have separate power pistons and fluid displacers. For the beta configuration the displacer and power piston are housed in the same cylinder. In gamma engines however, the power piston and displacer are in separate cylinders which leads to gamma type engines being physically larger than beta engines. Because of their compact multi-cylinder configuration, alpha type engines were explored by the automotive industry as high specific power outputs are possible [2].

In addition to different physical configurations, Stirling engines can further be divided into two groups based on their drive methods. In kinematic Stirling engines, manual linkages like cranks, connecting rods, or flywheels are used to move the working fluid through the

engine's cycle like that of a reciprocating engine. These engines use temperature-resistant seals around the piston which is exposed to high temperatures. This imposes strict requirements on the materials that can be used to make the seals to ensure high reliability. Unlike kinematic Stirling engines, free-piston engines use pressure variations in the working fluid to generate motion in the reciprocating components. In FPSE work is generally removed via the use of a linear alternator. Because FPSE have no manual linkages and they use clearance seals both the reliability and life expectancy of the engine are increased as there is no wear in the system. In a FPSE the mechanical dynamics and the thermodynamics are highly coupled while in kinematic engines, only the behavior of the working fluid is required to determine the performance of the engine as the dynamic phases are fixed by the mechanical linkages. This makes designing a FPSE more complicated as the performance of each individual component is tied to the other parts of the engine.

4. Free-piston Stirling engine design concepts

A schematic of a Stirling converter is shown in **Figure 1**. The key components are the hot heat exchanger, regenerator, cold heat exchanger, displacer, flexures, piston, and linear alternator. The first step in the design process is to use a one-dimensional thermodynamic modeling tool such as the Sage modeling software produced by Geodon Associates [5]. This model can be used to predict dimension of the Stirling engine components as well as the estimated performance of the engine. An example of the predicted performance variable from Sage is listed in **Table 1**. The estimated Stirling cycle efficiency (heat to work) is about 45%. The system efficiency (fuel to electricity) is around 38.3%.

After the initial sizes of the components are determined based on the power output of the engine being designed, a detailed examination of each component is conducted to ensure that the manufactured parts will meets the required operational life and to minimize conversion losses. There are various ways in which conversion losses occur in a Stirling engine [6] including flow separation, insufficient fluid travel distance, dead volumes, poor regenerator performance, thermal conduction losses, and shuttle and pumping losses. Many of these

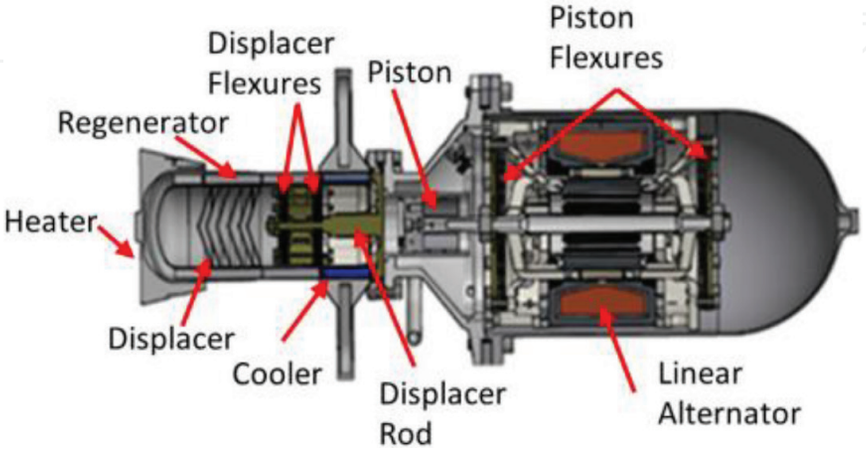

Figure 1. Stirling converter schematic.

Item	Value
Electrical power (W)	1215
Total thermal input (W)	3017
Parasitic loss/wall loss (W)	184
Heat rejection (W)	1493
Net cycle power (W)	1350
Stirling cycle efficiency (%)	44.74
Carnot efficiency (%)	71.01
Fraction of carnot (%)	63.00
Assumed alternator efficiency (%)	95.00
Burner efficiency (%)	90.00
System efficiency (%)	38.25

Table 1. Results of Stirling engine design analysis model.

losses are related to limitations in traditional manufacturing and can be alleviated by using additive manufacturing to produce a continuous heater head assembly. For example, thermal losses can be reduced by controlling the size of the gaps between components. As the size of the gaps is reduced the thermal losses decrease however if they become to small it leads to unwanted wear on both the moving and non-moving components resulting in a reduction in the expected lifespan of the convertor. The tolerance needed to achieve the optimal gap size requires high precision machining and often additional finish machining is required to obtain the desired fit. With traditional manufacturing, the components of the heater head assembly are joined using brazing or welding leading to added design change as their tolerance is hard to control. If an integrated design is produced via additive manufacturing, not only can the gap size between components be controlled but a smooth flow path between the heat exchangers and regenerator can be ensured while further reducing dead volumes.

4.1. Heater head assembly

A crucial component of a FPSE is the heater head assembly which consist of the hot heat exchanger, regenerator, pressure vessel, and cold heat exchanger. Historically the performance of Stirling engines was limited by the materials available. To achieve a long operational life of a FPSE, the hot end of the heater head assembly must withstand high temperatures and pressure over extended periods of time. Under these operating conditions, the reliability of the heater head assembly is influenced by the ultimate creep behavior of the material used. For operation at 810°C with an internal pressure of 3.3 MPa, the expected lifespan of the heater head would be limited if common metals are used because of their low tensile strength and creep resistance at high temperatures. Decreasing the operating temperature while increasing the life expectancy of the engine would vastly reduce the efficiency. Similarly, increasing the thickness of the heater head wall would also increase the life of the unit but it would lead to

an increase in axial conduction losses which also decreases the system's performance. Thus, the choice of an appropriate material with excellent creep resistance at high temperatures is critical to achieving both the desired performance and life expectancy of the designed FPSE. An evaluation of the use of various superalloys for the manufacturing of heater heads is presented in Ref. [7]. Finding a material that has all of the desired qualities is difficult. Alloys such as Udimet 720, IN 738LC, MA754, MarM-247, Inconel 718, and Inconel 625 are excellent candidates for use in high-temperature FPSE heater heads as they have high creep resistance and tensile strengths at high temperatures. However, they also have potential drawbacks such as post-weld cracking, welding difficulties, coarse grain recrystallization structures, and maximum temperature limitations.

In addition to the type of material used the type of heater head configuration used also is important. There are three types of heater heads commonly used in Stirling engines, monolithic, flat tubular, and vertical tubular heater heads, **Figure 2**. While monolithic heater heads are cheap and easy to manufacture, they have a limited heat flux and often used for small convertors. Both the flat tubular and vertical tubular configurations can have significantly higher heat fluxes. The flat tubular heater head design was used in solar Stirling engine applications. The high surface area and efficiency of the vertical U-shaped tubular heater head makes it ideal for use in larger Stirling convertors. The vertical tubes allow for easy integration with gas burners, however, using traditional manufacturing means, the reliability of the welded tube joints is low, and the associated manufacturing cost is high. The continued development of additive manufacturing would not only decrease the cost of a tubular heater head it would also increase the reliability as there would be no weld joints that are likely to fail.

4.1.1. Flow separation

A design drawback of a tubular heat exchanger design is the likelihood of jetting occurring at the outlet of the tubes. Flow separation between components is one of the major sources of conversion losses in a FPSE. Jetting at the exit of the hot heat exchanger not only increases

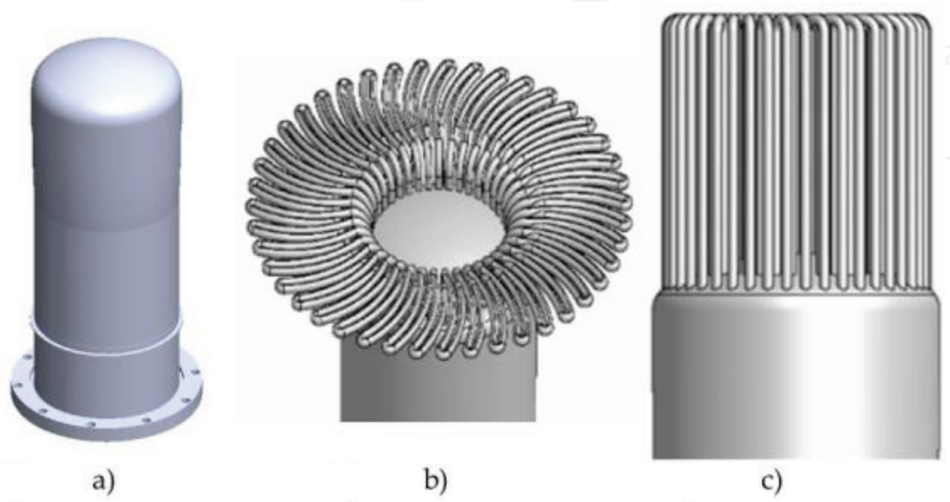

Figure 2. Different types of Stirling engine heater head configurations. (a) Monolithic, (b) flat tubular, (c) vertical tubular.

flow losses, it results in a reduction of the regenerator's performance. While the effects of jetting into the regenerator may be small for a random fiber regenerator where the flow can radially distribute within the regenerator, it is highly detrimental to the performance of a foil type regenerator where the flow in between foils cannot spread radially. Using computational fluid dynamics (CFD), the flow distribution between components can be analyzed and modification to the geometry can be suggested to ensure a smooth flow transition between components. For example, an internal diffuser was designed to eliminate the effects of jetting for a 1 kW tubular heater head along with a comparison of the flow distribution, **Figure 3**. The addition of the diffuser in the plenum space between the hot heat exchanger and the regenerator increases the Stirling convertors efficiency although there are added flow losses across the diffuser. This simulation verifies the idea that the integrated design will minimize the flow losses and maximize the thermal efficiency.

4.1.2. Dead volume analysis

Using additive manufacturing to reduce the thermal losses are possible by reducing the dead volumes between the heat exchangers and regenerator through controlling the size and shape of these plenum spaces. Dead volumes are areas that are un-swept by either the power piston or displacer and occur in the generator, cooler, heater and all clearance spaces. Passive dead volumes are areas that do not take part in the volumetric expansion-compression cycle, which decrease the overall cycle efficiency. A detailed analysis of the impact of dead volumes in an entire Stirling engine is presented by Ref. [8]. In the heater head assembly, dead volumes occur in the hot space and expansion space. In the hot space area, the dead volume occurs in the knuckle section, **Figure 4a**. In traditional Stirling engine design when using a tubular type heat exchanger, the heater tubes penetrate through the pressure vessel wall and extend to the top of the regenerator. The portion of the heat exchanger tubes inside the pressure vessel do not act as part of the heat exchanger and only function to reduce the dead volume of the working gas. However, the volume inside the extended heater tube section still acts as dead volume. The size of this dead space is related to the length of the extended heater tubes inside of the pressure vessel which depends on the knuckle (R_k) and dome (R_D) radii, **Figure 4a**. As

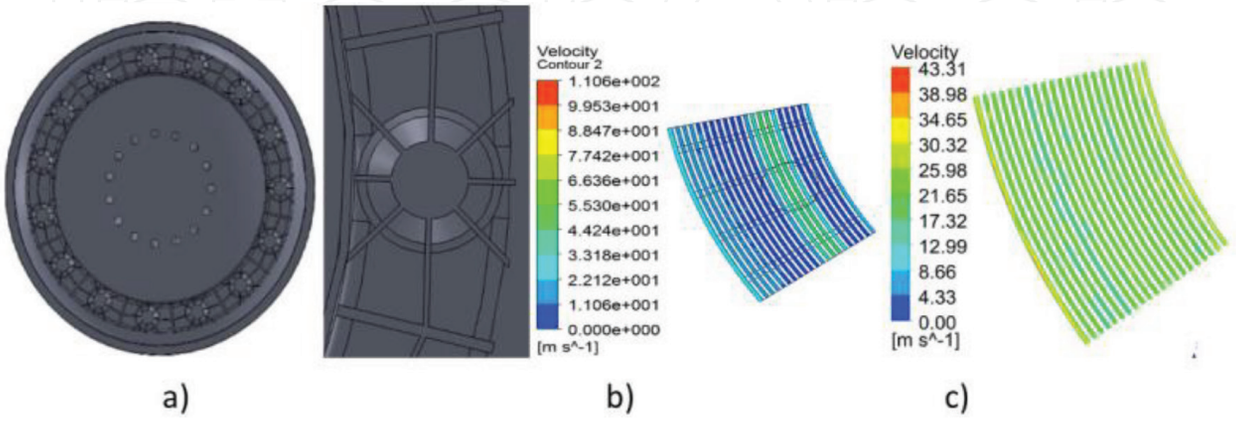

Figure 3. a) Designed diffuser plate and velocity distribution in a foil regenerator b) without and c) with the diffuser.

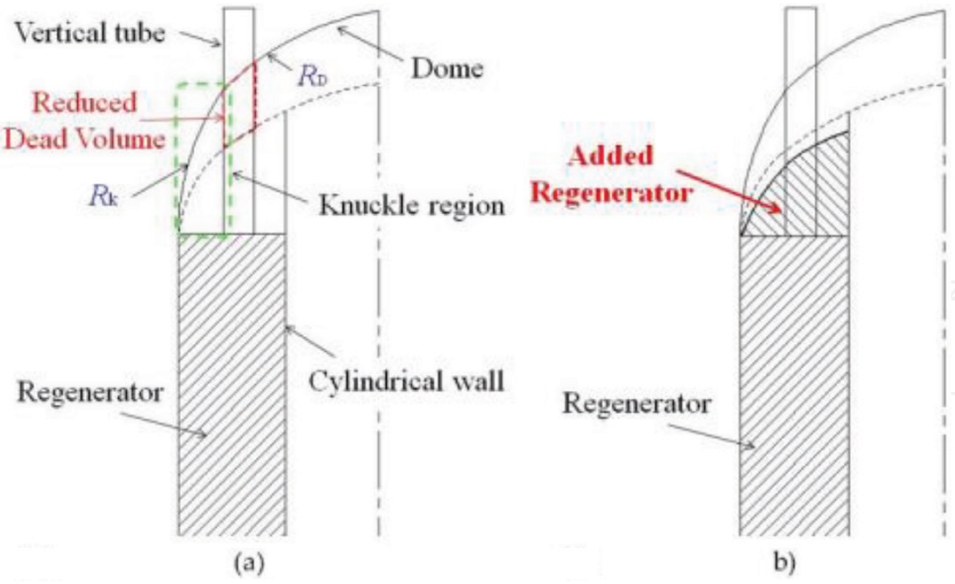

Figure 4. Dead volume in the hot space of heater head. (a) Knuckle and dome sections, (b) curved section of regenerator.

the dome radius is increased and the knuckle radius decreased the dome or cap of the heater head flattens. This reduces the length of the extended heater tubes, thus decreasing the dead volume. Ideally, the dome radius would be increased and the knuckle radius decreased until the dead volume was eliminated, however this leads to a stress concentration in the knuckle region from the high temperatures and pressures. A potential solution to reduce the stress is to increase the thickness of the wall in the knuckle region, but this results in an increase in axial conduction losses. Thus, the geometry of the knuckle and dome region must be optimized to balance axial conduction loses, localized stress, and dead volume. An alternative means of reducing the dead volume in the knuckle region is to add a curved section to the top of the regenerator to fill the knuckle region, **Figure 4b**. This method of dead volume reduction has never been employed before as manufacturing of the complex geometry was difficult and costly with traditional manufacturing methods. However, additive manufacturing can be employed to effectively create a complex regenerator geometry.

4.1.3. Stress analysis

Another major design challenge is the thickness of the pressure vessel wall. The heater head assembly not only experiences high pressures, but also a large thermal gradient. Therefore, the design is always a balance between minimizing thermal losses while maintaining structural integrity. Finite element analysis (FEA) is a useful tool to evaluate the stress within the heater head pressure vessel to ensure the parts will not fail. The pressure vessel of a FPSE heater head is generally designed using Section VIII Division 2 of the ASME Boiler and pressure vessel design code [9]. A coupled thermal and structural analysis out to be conducted to evaluate both the primary and secondary stresses in the heater head. An example of the resulting pressure distribution of a tubular heater head for a 1 kW FPSE is shown in **Figures 5** and **6** along with the employed boundary conditions. A zero-displacement boundary condition is applied

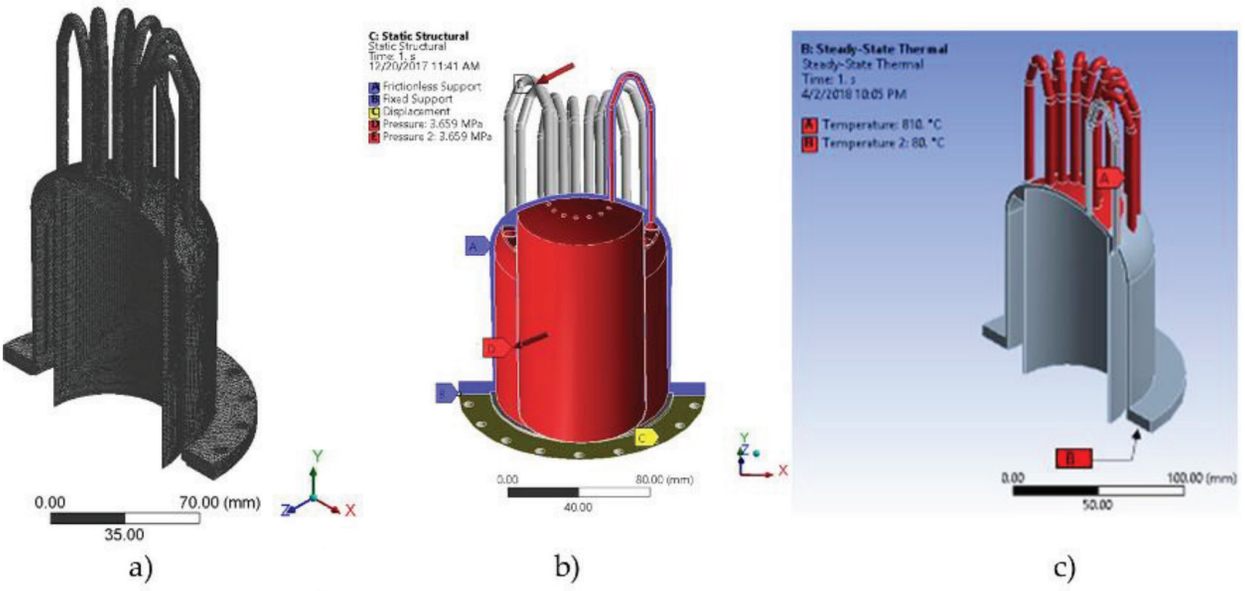

Figure 5. Heater head thermal and structural boundary conditions.

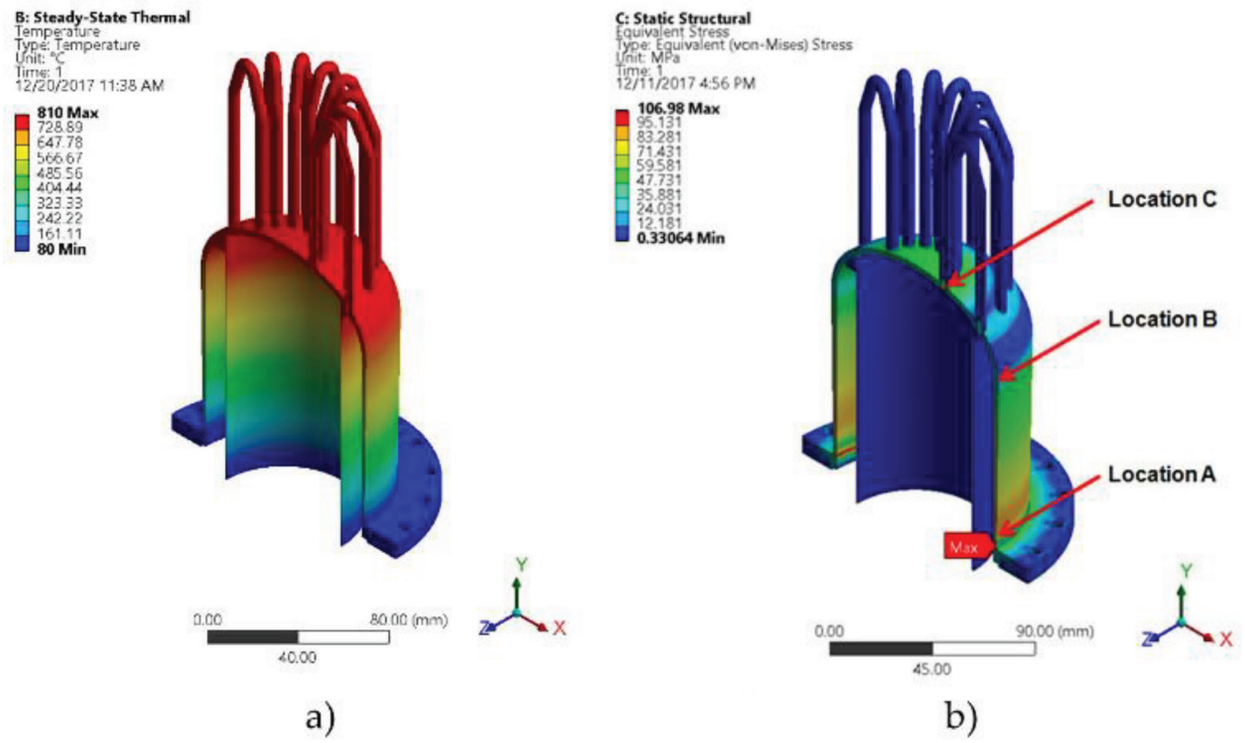

Figure 6. Temperature distribution and stress contours of heater head.

to the bottom surface of the heater head to prevent translation. Frictionless supports are used to mimic the symmetry in the system. A pressure of 3.66 MPa is applied to the internal surfaces of both the pressure vessel and tubular hot heat exchanger. For the thermal model, the bottom portion of the heater head assembly is set to 80°C and the outer surface of the hot heat exchanger tubes has an applied temperature of 810°C. The largest stress occurs at the bottom

flange and is 106.9 MPa at a temperature of 115°C. This is below the 238 MPa allowable stress of the material. Additionally, the membrane stresses at Location B & C are 36.6 and 32.8 MPa. The temperatures at these locations are 716 and 810°C respectively with allowable stresses of 198 and 84 MPa. Therefore, the stresses in the heater head assembly under peak operating pressure and temperature are acceptable based on ASME boiler codes as positive safety margins are obtained. Based on the creep and rupture life properties of Inconel 625, for the designed presented at locations C it would take over 6000 hours to reach an estimated 2% creep. The estimated rupture-life at location C is over 200,000 hours. For location B both the estimated creep and rupture-life are significantly higher in comparison to location C because of the lower temperature at location B.

4.1.4. Conduction losses

Axial conduction losses also contribute to conversion losses in a FPSE. As previously mentioned the axial conduction losses must be balanced with the allowable stress distribution and dead volumes. The conduction losses in the heater head assembly wall can be significant as it experiences a large thermal gradient. Minimizing the thickness of the displacer cylinder wall is only limited by the capabilities of additive manufacturing as there is equal pressure on both sides of the wall. Minimizing the thickness reduces axial conduction losses, therefore a thickness of 0.5 mm can be used based on the limitations of the state of the art in additive manufacturing. The outer wall of the heater head however does experience a large difference in pressure between the inner and outer surfaces. This wall is significantly thicker. As the axial conduction losses are a significant source of parasitic losses in a FPSE, every effort should be made to minimize the wall thickness. **Figure 7** shows four types of wall profiles often used. Steady state thermal models of the heater head can be used to estimate the conduction losses. The same boundary conditions used in the coupled thermal-structural model were used, **Figure 7**. In all the cases the thickness of the heater head dome and cap are kept the same as it is decided based on the allowable creep stress at the operating temperature. The thickness at the cold end can also be decided based on the local allowable stresses at the rejection temperature. Since this temperature is significantly lower the allowable stress is higher and this wall thickness is much smaller. In the single taper case, the thickness of the wall varies

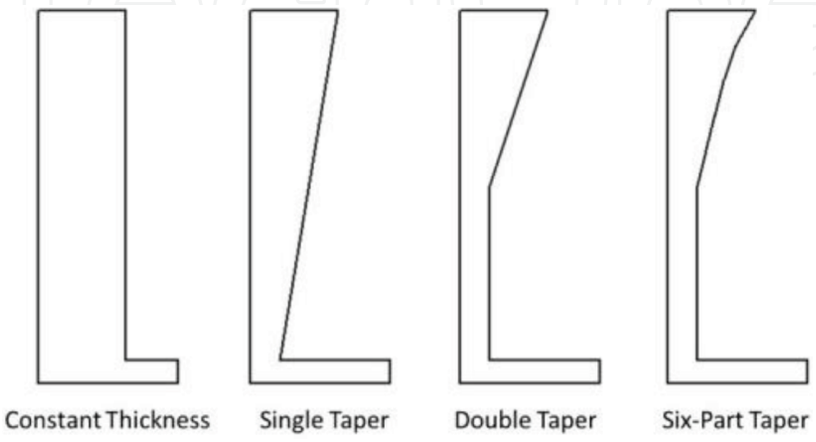

Figure 7. Heater Head Wall configurations.

linearly from the hot end (top) to the cold end (bottom). For the double taper, the thickness still linearly decreases however it reaches the minimum thickness at the midpoint of the wall and then remains constant. The six-part taper has five concave curves that decrease the thickness from the top to the middle.

The temperature distribution along the heater head wall varies based on the geometry examined (**Figure 8**). A nearly linear profile occurs for the constant wall thickness case. For the other cases considered a non-linear profiles forms. The non-linearity of the curve increases from the single to double to 6-part taper. The estimated axial conductions losses for the cases shown are listed in **Table 2**. The constant wall thickness case has the highest conduction losses, 83 W. Using a single taper results in a 23% reduction in the axial conduction losses compared to the constant wall thickness. If the cross-sectional area of the heater head wall is further reduced by using a double taper the conduction losses decrease an additional 4%. The 6-part tapper has the lowest conduction losses of the four cases shown.

4.2. Regenerator

The regenerator is crucial to the efficiency of a FPSE [10]. The regenerator acts as a means of temporary energy storage and is located between the hot and cold heat exchangers. When the working fluid travels from the hot heat exchanger to the cold heat exchanger, it transfers a portion of its energy to the solid regenerator medium. When the flow travels back from the cold to hot heat exchanger, it retrieves the energy from the regenerator. Various types of regenerators have been investigated to improve the heat transfer and achieve a high storage capacity. The types of regenerators investigated include woven screens, random fibers,

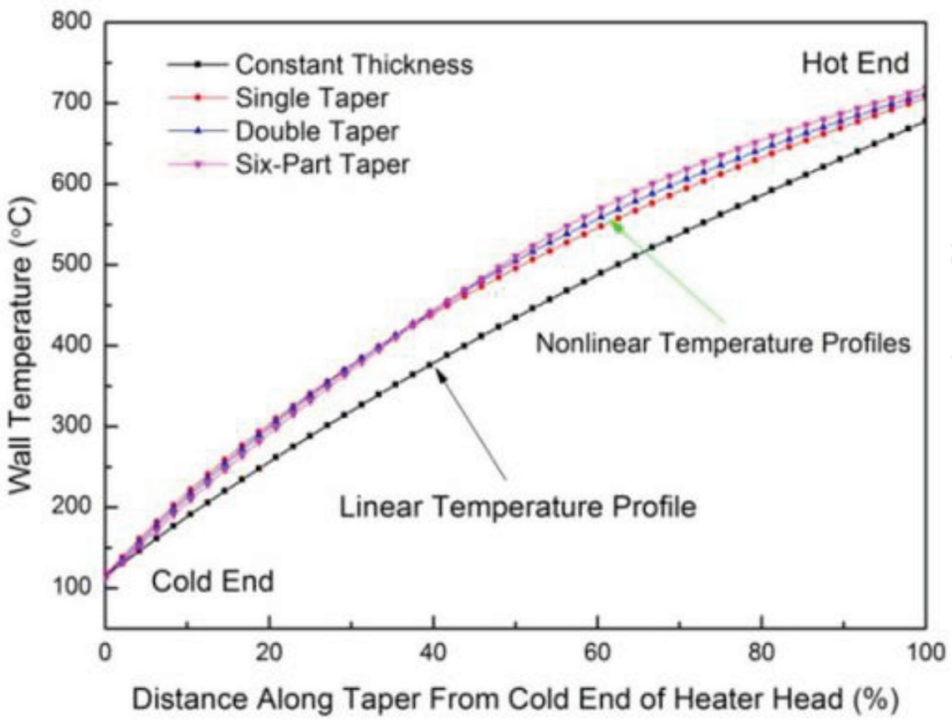

Figure 8. Temperature profile in the heater head wall.

Taper profile	Conduction loss (W)
Constant thickness	82.9
Single taper	63.7
Double taper	60.3
Six taper	54.7

Table 2. Conduction loss results for heater head taper configurations.

wrapped-foils, and segmented-involute foils [11]. Theoretically, a foil regenerator would have the best performance as it has the highest possible figure of merit which is the ratio of the heat transfer coefficient to the friction coefficient. However, because it is nearly impossible to manufacture a robust foil regenerator they are seldom used in FPSE. Using traditional manufacturing techniques, foil regenerators are made by wrapping the foils layer by layer using pre-formed dimples on the foils for spacing, **Figure 9a**. Because the performance of a foil regenerator is directly dependent on the spatial structure of the foils. If the foil spacing changes, the performance dramatically reduces. Unfortunately, due to thermal expansion during thermal cycles, the foil spacing changes within a short period because foils are not well connected and supported. This change leads to flow redistribution and a severe decrease in regenerator effectiveness. Therefore, FPSE manufactures use a less efficient albeit more reliable regenerator to ensure consistent operation. Although woven screen regenerators can be manufactured with high reliability there is a limit on their porosity which limits the maximum engine performance possible [12]. Random fiber regenerators are not limited by porosity, but their effectiveness is lower as they have a smaller area to volume ratio and significantly higher flow losses compared to foil regenerators. **Figure 9b** shows a random fiber regenerator.

Using additive manufacturing methods, a robust foil regenerator can be fabricated that has the same high reliability as a mesh screen regenerator while having superior heat transfer characteristics and minimal flow losses. The thin foils of the regenerator are ingeniously interconnected to increase the rigidity of the regenerator and maintain uniform foil spacing at high temperatures. The current state of the art in additive manufacturing has a limit on the minimum thickness based on the nominal diameter of the powder metals used. Currently the minimum foil thickness is 0.3 mm. Webs are designed to strengthen the regenerator and to keep the foil spacing unchanged. The designed regenerator is shown in **Figure 10**. There is a curved section at the top of the regenerator that is designed to fit into the space between the knuckle wall and displacer cylinder wall of the heater head to reduce the detrimental dead volumes. A ring is also added to the bottom of the regenerator to both add extra support and to fix the regenerator's axial location in the heater head assembly.

Using FEA, the robustness of the regenerator is investigated. A temperature of 810°C is applied to the top of the regenerator foils and a temperature of 80°C is applied to the bottom surface, **Figure 11**. For the structural model, the bottom edge of the outer ring is fixed to prevent the regenerator from translating, additionally, frictionless supports are applied to the symmetry planes. Because of the novel design of the regenerator, the only stress that occurs are thermally induced. The maximum stress, axial deformation, and radial deformation of

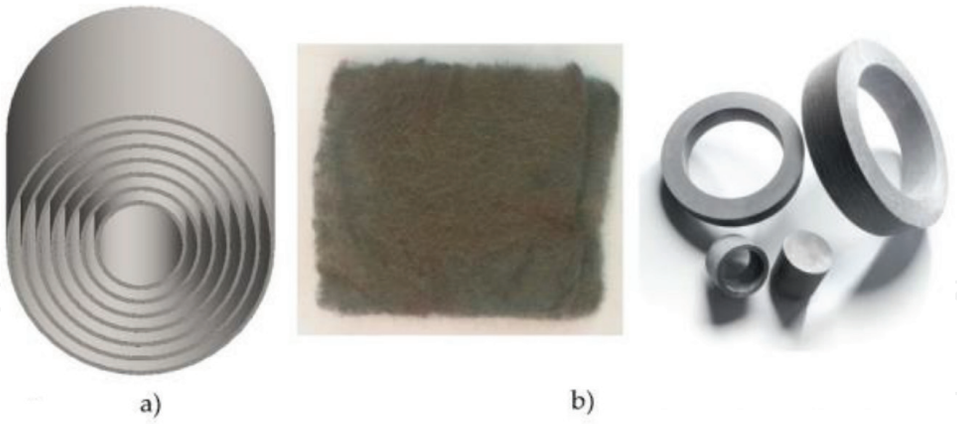

Figure 9. Wrapped foil and random fiber regenerators.

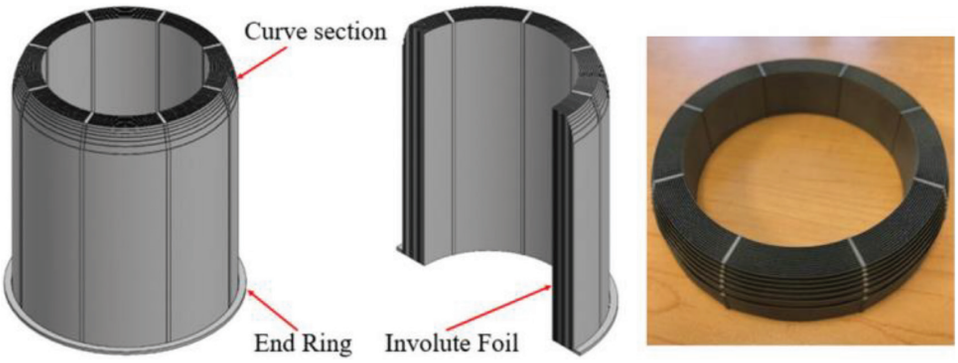

Figure 10. Involute foil regenerator.

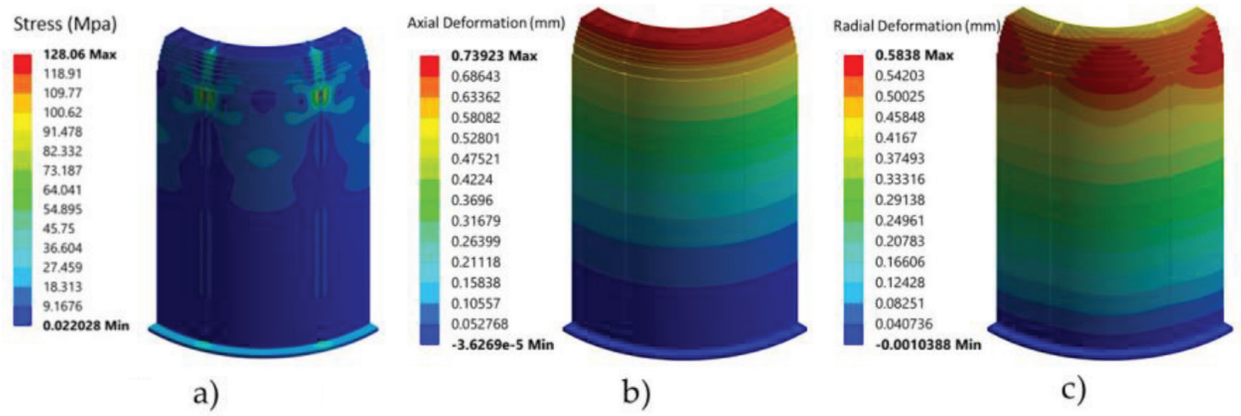

Figure 11. Stress distribution, axial and radial deformation of the involute regenerator.

the regenerator are shown in **Figure 11**. The maximum stress occurs in the outer foils near the regenerator ribs. This stress is well below the yield stress of Inconel 718 even at high temperatures leading to large margins of safety. The foils radially deform a maximum of 0.6 mm although this level of deformation may seem detrimental, there is only a 0.01 mm maximum deformation between foils. Therefore, the spacing between the foils remains constant even

at high temperatures. Thus, additive manufacturing can be used to produce a robust foil regenerator that can achieve the theoretically high figure of merit and vastly improve the performance of modern FPSE.

4.3. Heat exchangers

The hot heat exchanger in this study is a tubular type heat exchanger which has high heat transfer effectiveness while also exhibiting good fuel source integration capabilities. Using traditional manufacturing techniques, the heat exchanger tubes are bent and then welded to the pressure vessel. This can lead to numerous potential areas where leaks can form, thus the reliably of tubular heat exchangers are low. However, using additive manufacturing, the tubular heat exchanger and pressure vessel can be printed as one continuous part eliminating potential leaks and greatly increase the reliability. Additionally, the geometry of the tubes can be manipulated to further improve heat transfer with the chosen fuel sources burner. **Figure 12b** shows a tubular heater head where one end of the tube is extended through the knuckle region of the heater head and the other is connected to the dome of the pressure vessel. The diameter and length of the tubes are dependent upon the desired FPSE power output and the fuel combustor used. The heat exchanger shown in **Figure 12** has 15 U-shaped tubes with an internal diameter of 2.5 mm. However, the shape of the tube can be manipulated based on the feedback from additive manufactures and to increase the heat transfer, **Figure 5**. Furthermore, novel flow guides were used to increase the convective heat transfer around the tubes to further improve the system efficiency. The design of the burner interface with the hot exchanger is critical to the performance of the engine. A detailed description and numerical simulation of the flow guides and burner interface for the enhancement of heat transfer is available in Ref. [13]. An example of the combustion gas distribution is also seen in **Figure 12c**.

A fin-type heat exchanger is commonly used for the cold heat exchanger because of its low-cost and manufacturability (**Figure 13**). Extrusion or casting can be employed for the manufacturing of the fin heat exchangers. The dead volume can be reduced as well as minimizing flow separation by adding a curved section to the bottom of the heat exchanger. Usually a

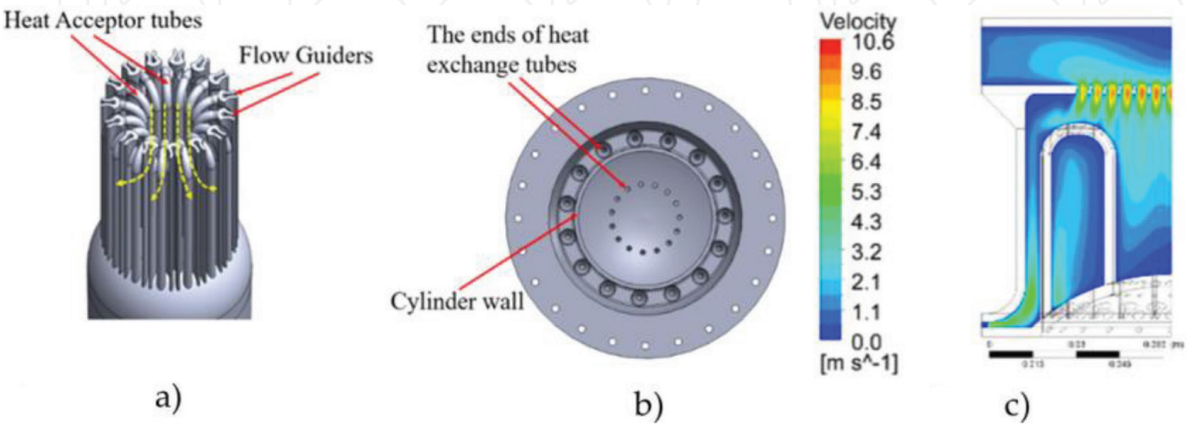

Figure 12. a) Tube bundle of tubular heat exchanger and (b) layout of tubular heat exchanger tubes and (c) combustion gas flow distribution.

highly conductive material such as copper is used for the cold heat exchanger to improve the heat transfer. The temperature difference between the coolant and the working gas in the cold heat exchanger is significantly smaller than that seen in the hot heat exchanger therefore the cold heat exchanger is typically larger compared to the hot heat exchanger.

4.4. Displacer assembly

The displacer assembly can also be evaluated using FEA to examine the resulting stress distribution. An example displacer assembly is shown in **Figure 14a**. Inconel 625 is used for the displacer cap while stainless steel 304 is used for the remaining parts. The thermal and structural boundary conditions are shown in **Figure 14b–d**. The top and bottom surface are set to 810 and 80°C, respectively. A 332.6 kPa pressure was applied to the outer surfaces of the displacer assembly. This is roughly 10% of the charge pressure. Additionally, a hydrostatic pressure load was applied to the displacer rod cylinder to mimic the pressure gradient from 332.6 kPa to 0 Pa. Again, frictionless supports are used to simulate the symmetry present in the system. Lastly,

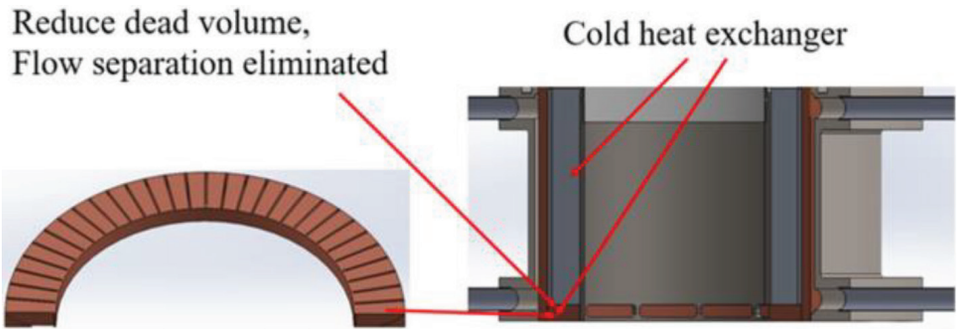

Figure 13. Cold heat exchanger.

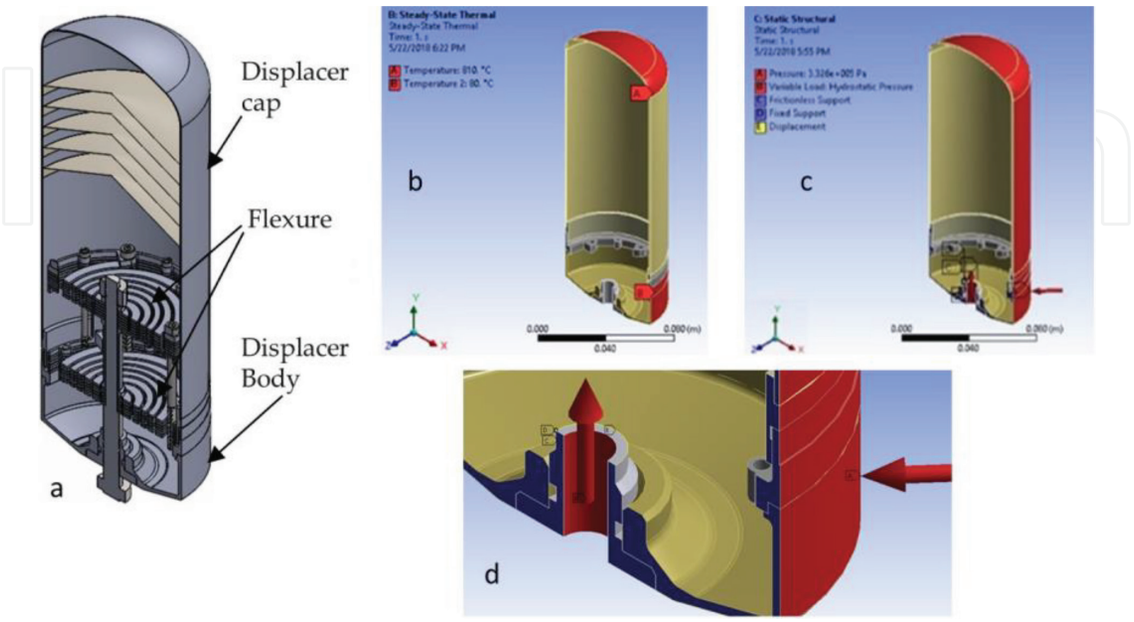

Figure 14. a) Displacer assembly, b) thermal, c) structural boundary and d) structural load at displacer body.

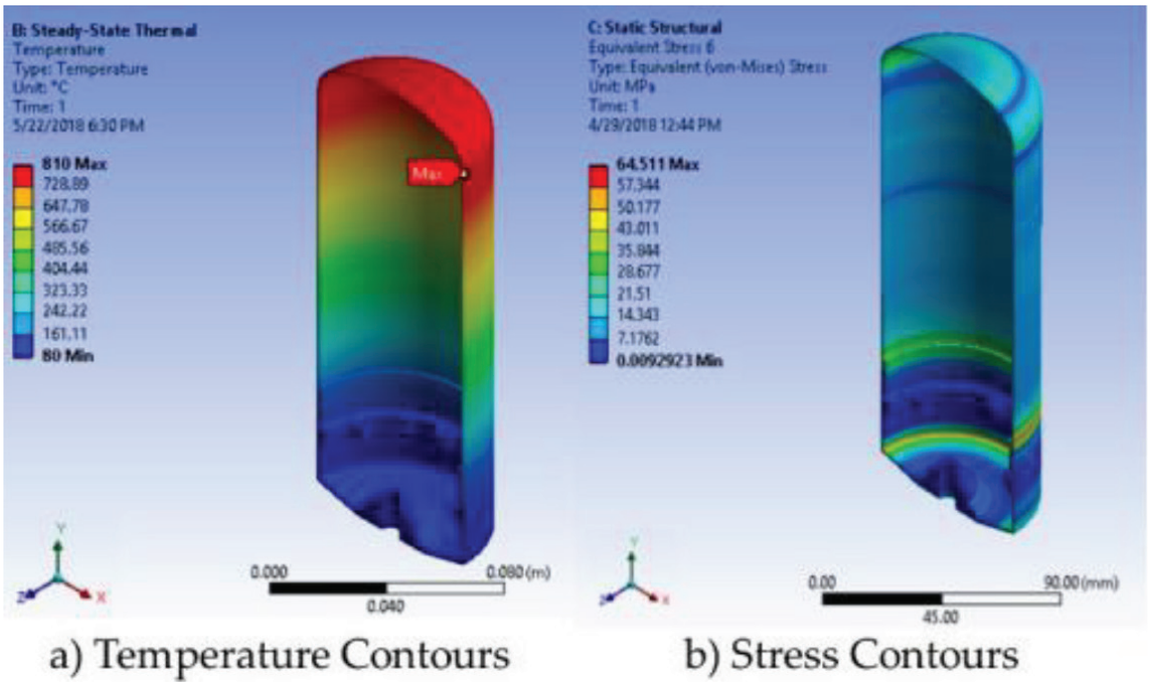

Figure 15. Temperature distribution and stress contours of displacer assembly.

fixed supports are applied to the faces where the flexures are connected to the displacer assembly. The predicted temperature and stress distributions are shown in **Figure 15**. The maximum stress of 64.5 MPa occurs at the interface between the displacer cap and the displacer body connector. The allowable stress for Inconel 625 at 90°C is 184 MPa. In addition to the maximum stress in the entire assembly, the maximum and membrane stresses for the individual displacer assembly parts has to be evaluated. In all cases both the maximum and membrane stresses shall stay below the allowable stresses at the corresponding part temperature with high margins of safety and to ensure that displacer design is acceptable and will have the desired operational life.

5. Dynamic analysis

5.1. Dynamic analysis of displacer assembly

In FPSE the cyclic motion of the working fluid is driven by the displacer. Both the displacer configuration and dynamics are critical to the performance of the engine, thus during the design of a FPSE, a dynamic analysis of the displacer assembly must be conducted. This analysis is used to figure out the required number of flexures to obtain the desired motion. A mass-spring diagram of the displacer is given in **Figure 16** along with a vector force polygon. An equation for the motion of the displacer is given in Eq. 1.

$$M_d \vec{\ddot{x}}_d = A_r \vec{P}_c + K_d \vec{x}_d + K_s \vec{x}_d + A_d\left(\vec{P}_c - \vec{P}_e\right) + D_d \vec{\dot{x}}_d \tag{1}$$

where x_d is the displacer motion, X_d is the amplitude of the displacer, X_p is the piston amplitude, Φ_m and Φ_p are the phase angle of the displacer and piston, A_r and A_d are the displacer

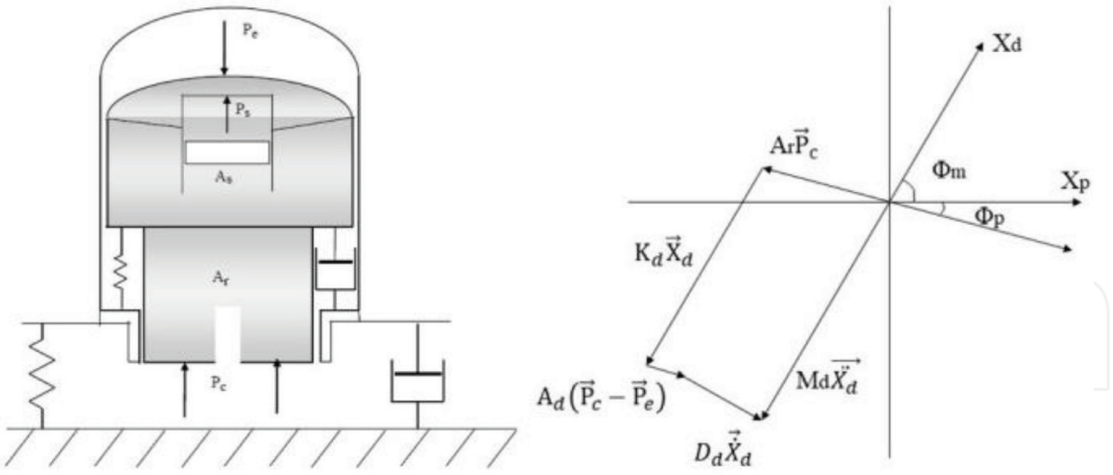

Figure 16. Dynamics of Stirling engine and displacer vector diagram.

road and frontal area, P_c and P_e are the pressure amplitude in the compression and expansion spaces, D_d is the displacer damping coefficient, M_d is the total moving mass, K_d is the total axial spring rate of the displacer flexures, $\vec{\dot{x}}_d$ is the displacer velocity, and $\vec{\ddot{x}}_d$ is the displacer acceleration. The velocity of the displacer assembly is calculated using Eq. 2.

$$\dot{x}_d = X_d \omega \cos(\omega t) = X_d \omega \sin\left(\omega t + \frac{\pi}{2}\right) \tag{2}$$

This is a harmonic function with the same frequency as the displacement and an amplitude ω times as large. The velocity is 90° out of phase with the displacement. The acceleration of the displacer assembly is given by Eq. 3:

$$\ddot{x}_d = -X_d \omega^2 \sin(\omega t) = X_d \omega^2 \sin(\omega t + \pi) \tag{3}$$

The acceleration is 180° ahead of the displacement with a ω^2 times larger amplitude. The remaining parameters listed in Eq. 1 are determined based on the one-dimensional thermodynamic model Sage. The main reason the dynamic analysis is conducted is to determine the number of flexures required. Based on the parameters for a 1 kW engine used as a case study here, a total of 8 flexures is needed. However, the natural frequency of the number of the system is considered as well. Thus, based on variations in fabrication and uncertainties a total of 10 flexures shall be chosen. A rocking mode analysis is used to determine the natural frequency of the system rocking mode to ensure that it is far from the operating frequency. In this system for 10 flexures, the frequency is 159 Hz this is far from the operating frequency of 60 Hz and its multiples. Therefore, the use of 10 flexures is acceptable.

5.2. Rocking mode analysis

The rocking mode of the displacer out to be analyzed to ensure that it is not close to the operating frequency or its harmonics. If it is, it can result in rubbing of the displacer on the pressure vessel inner wall leading to unwanted wear and a decrease in lifespan (**Table 3**). The rocking mode analysis is also used to determine the height between flexure stacks and verify the

Numbers of Flexure	Total Moving mass m (Kg)	*a* (m)	*b* (m)	K_r (N/m)	f_n(Hz)
10	0.931	0.01693	0.0093	2,225,346	158.6

a: the distance from spring to wheel base, b: the distance from spring to displacer center of gravity, K_r: flexure radial spring rate, f_n: rocking frequency

Table 3. Calculated model frequencies.

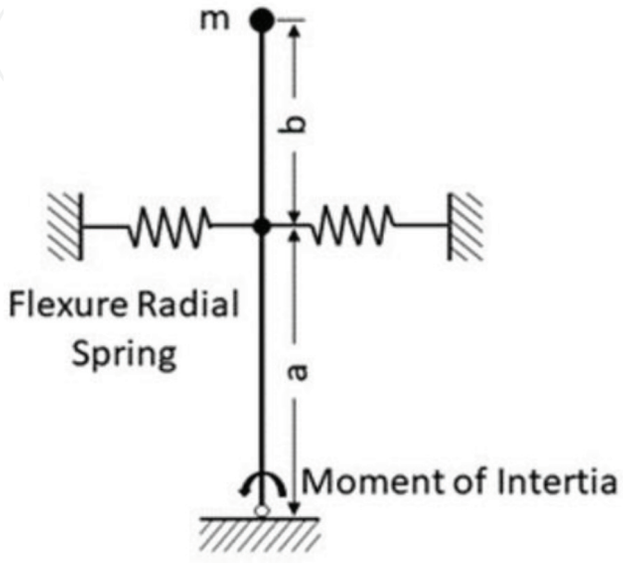

Figure 17. Displacer assembly rocking mode.

quantity from the dynamic analysis. As seen in **Figure 14a**, the flexures are separated into two stacks. Each stack consisted of five flexures. A schematic of the rocking mode analysis is depicted in **Figure 17**. The rocking or natural frequency is determined using Eq. 4.

$$f_n = \frac{1}{2\pi}\frac{\sqrt{a^2 k_r - mg(a+b)}}{m(a+b)^2} \tag{4}$$

where *a* is the distance between the flexure stacks centers and wheelbase, *b* is the distance between the center of gravity of displacer assembly and flexure stacks centers, K_r is the total radical spring rate of the flexures, *m* is the total moving mass of displacer assembly, and *g* is the gravity of earth. The predicted natural frequency of the displacer assembly using two stacks of 5 flexures is 159 Hz. This is not only far from the operating frequency of 60 Hz it is also far from its harmonics (120 and 180 Hz). Therefore, excess rocking of the displacer is unlikely to occur under the given operating conditions.

6. Performance specifications

The final step in the design of a FPSE is to map the performance of the engine over an operating frequency range. For example, if the design operation is at 60 Hz the performance should be mapped in the 50–70 Hz range. Examining the performance of the engine over

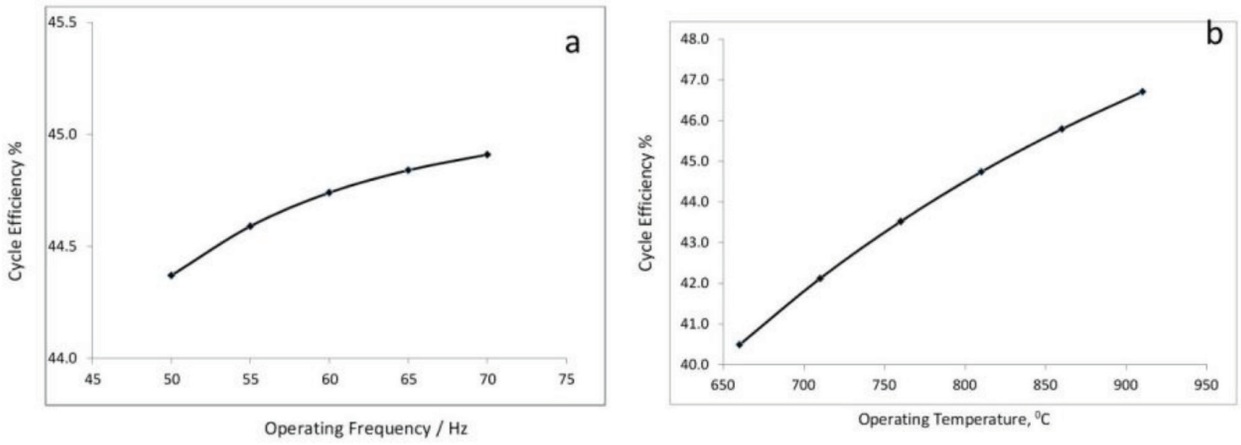

Figure 18. Frequency and temperature mapping of a FPSE.

a frequency range indicates that the efficiency of the system can be increased by increasing the operating frequency (**Figure 18a**). Generally speaking as the operating frequency increases both the efficiency and power density also increase [14]. For low power engines the frequency is limited to 80 Hz while for high power engines the operating frequency does not exceed 60 Hz. The limitations on operating frequency are due to the high velocities that can occur in the heat exchanges and regenerators with high frequencies, limited flexure spring forces for a given geometry, and the proximity to grid power of 60 Hz. In addition to performance mapping over the frequency, mapping over a range of temperatures should also be performed. The performance of a FPSE at various temperatures is shown in **Figure 18b**. As the operating temperature increases the efficiency of the system also increases. By increasing the temperature from 660–910°C an increase in system efficiency of 5.32% is possible. Note that these does not consider any potential conversion losses that can occur due to the potentially thicker walls required to counteract the allowable creep stress at high temperatures.

7. Conclusion(s)

The design analysis of a FPSE was presented. The key components including the heater head pressure vessel, regenerator, hot and cold heat exchangers, and displacer are discussed. FPSE are ideal for use in various power conversion applications. In addition to the design constraints and approaches of various components, dynamic and rocking mode analyses of the engine are also presented. Manufacturing of an integrated pressure vessel and heat exchanger assembly enables a new degree of control over conversion efficiency. Additionally, CFD and FEA can be used to further reduce axial conduction losses and flow separation to increase efficiency. Additive manufacturing is not just limited to the manufacturing of the heater head, it can be used to generator a robust foil regenerator that will have the highest figure of merit possible to further increase the systems efficiency. Therefore, the use of emerging manufacturing techniques can help to achieve higher system efficiency, better reliability, and enhanced robustness while reducing the cost.

Acknowledgements

This project was conducted under United State DOE ARPA-E contract, DE-AR0000864. Authors would like to express their appreciation to DOE ARPA-E for the financial support.

Conflict of interest

The authors declare no conflict of interest.

Nomenclature

X_d	displacer amplitude
Xp	piston amplitude
Ar	displacer rod area
A_d	displacer frontal area
D_d	displacer damping coefficient
K_d	$N*K_{axial}$, total axial spring rate of displacer flexure
$\ddot{x}_d$	acceleration of the displacer
K_r	radial spring rate of displacer flexure
S_y	yield stress
S_u	ultimate stress
CHP	combined heat and power
BPV	boiler and pressure vessel
Φ_m	phase angle of displacer motion
Φp	phase angle of dynamic pressure in compression space
P_c	dynamic pressure amplitude in compression space
P_e	dynamic pressure amplitude in expansion space
M_d	total moving mass of displacer assembly
N	quantity of displacer flexure
K_{axial}	axial spring rate of displacer flexure
f_n	displacer rocking mode frequency

S_m	allowable stress
S_{creep}	creep stress
FPSE	free-piston Stirling engine
FEA	finite element analysis

Author details

Songgang Qiu* and Laura Solomon

*Address all correspondence to: songgang.qiu@mail.wvu.edu

Department of Mechanical and Aerospace Engineering, West Virginia University, Morgantown, USA

References

[1] Abbas M, Boumeddane B, Said N, Chikouche A. Dish Stirling technology: A 100 MW solar power plant using hydrogen for Algeria. The International Journal of Hydrogen Energy [Internet]. 2011 Apr;**36**(7):4305-4314. Available from: http://linkinghub.elsevier.com/retrieve/pii/S0360319910024997

[2] Renzi M, Brandoni C. Study and application of a regenerative Stirling cogeneration device based on biomass combustion. Applied Thermal Engineering. 2014;**67**(1):341-351

[3] Magri G, Di Perna C, Serenelli G. Analysis of electric and thermal seasonal performances of a residential microCHP unit. Applied Thermal Engineering [Internet]. 2012 Apr;**36**(1):193-201. Available from: http://linkinghub.elsevier.com/retrieve/pii/S1359431-111006533

[4] Hsu ST, Lin FY, Chiou JS. Heat-transfer aspects of Stirling power generation using incinerator waste energy. Renewable Energy [Internet]. 2003 Jan;**28**(1):59-69. Available from: http://linkinghub.elsevier.com/retrieve/pii/S0960148102000186

[5] Gedeon D. Sage Stirling-Cycle Model-Class Reference Guide. 11th ed. Athens, OH: Gedeon Associates; 2016

[6] Tanaka M, Yamashia I, Chisaka F, Yamashita I, Chisaka F. Flow and heat transfer characteristics of the Sritling engine regenerator in an oscillating flow. JSME International Journal. 1990;**33**(2):283-289

[7] Bowman R, Ritzert F, Freedman M. Evaluation of candidate materials for a high-temperature Stirling convertor heater head. In: AIP Conference Proceedings. AIP; 2004. pp. 821-828

[8] Puech P, Tishkova V. Thermodynamic analysis of a Stirling engine including regenerator dead volume. Renewable Energy [Internet]. 2011 Feb 1 [cited 2018 May 21];**36**(2):872-878. Available from: https://www.sciencedirect.com/science/article/pii/S096014811000337X

[9] Boiler and Pressure Vessel Code–2010 Edition. New York, NY: ASME; Retrieved 9 November 2011

[10] Kongtragool B, Wongwises S. A review of solar-powered Stirling engines and low temperature differential Stirling engines. Renewable and Sustainable Energy Reviews [Internet]. 2003 Apr;**7**(2):131-154. Available from: http://www.sciencedirect.com/science/article/pii/S1364032102000539

[11] Ibrahim MB, Tew RC Jr. Stirling Convertor Regenerators. Boca Raton: CRC Press; 2012

[12] Zhao TS, Cheng P. Oscillatory pressure drops through a woven-screen packed column subjected to a cyclic flow. Cryogenics (Guildf). 1996;**36**(5):333-341

[13] Costa S-C, Tutar M, Barreno I, Esnaola J-A, Barrutia H, García D, et al. Experimental and numerical flow investigation of Stirling engine regenerator. Energy [Internet]. 2014 Aug [cited 2017 Jul 24];**72**:800-812. Available from: http://linkinghub.elsevier.com/retrieve/pii/S0360544214006975

[14] Urieli I, Berchowitz DM. Stirling Cycle Engine Analysis [Internet]. A. Hilger; 1984. 256 p. Available from: https://books.google.com/books?id=d9pSAAAAMAAJ

IntechOpen